Indonesian Physical Review
Volume 08 Issue 01, January 2025
P-ISSN: 2615-1278, E-ISSN: 2614-7904

Modeling Influence of Urban Sprawl on Urban Heat Island (UHI) Activity in Kolaka Regency

Satriawan Nadhrotal Atsidiqi[1,2*], Eko Hadi Sujiono[1*], Husain[1]
[1] *Department of Physics, Faculty of Mathematics and Natural Sciences, Makassar State University, Indonesia*
[2] *Sangia Ni Bandera Meteorological Station, Indonesian Agency for Meteorology, Climatology, and Geophysics, Indonesia*

[*]*Corresponding Authors E-mail: satriawan.atsidiqi@bmkg.go.id, e.h.sujiono@unm.ac.id*

Article Info

Article info:
Received: 28-08-2024
Revised: 29-10-2024
Accepted: 13-12-2024

Keywords:
Urban Sprawl; UHI; WRF; BIG; Verification

How To Cite:
S. N. Atsidiqi, E. H. Sujino, Husain, "Modeling Influence of Urban Sprawl on Urban Heat Island (UHI) Activity in Kolaka Regency", Indonesian Physical Review, vol. 8, no. 1, p 162-180, 2025.

DOI:
https://doi.org/10.29303/ipr.v8i1.385

Abstract

The expansion of urban areas into rural regions, known as Urban Sprawl, contributes to the Urban Heat Island (UHI) phenomenon, where urban areas exhibit higher temperatures than their rural counterparts. Kolaka Regency is an area with significant potential for Urban Sprawl and subsequent UHI activity. Therefore, it is essential to investigate the impact of Urban Sprawl on UHI in the Kolaka region. This study simulates these changes using the Weather Research and Forecasting (WRF) model, incorporating land cover data from the Geospatial Information Agency (BIG) with four urban schemes: SLUCM, BEM, and the default non-UCM/land cover. The simulation also includes the Kolaka 2042 development map for Urban Sprawl projections. Simulations were conducted over 48 non-rainfall events across 12 months. The results indicated that the WRF BIG-BEM model demonstrated the highest verification accuracy and the lowest errors, with a MAPE of 4.70%, CRMSE of 1.06°C, and a correlation coefficient of 87.62%. Including BIG land cover and the BEM urban scheme enhanced the model's performance, with a MAPE of 17.92%, CRMSE of 10.11%, and a correlation improvement of 3.18%. The UHI effect predominantly ranged from -2.0 to 2.5°C, with the highest values observed in the Pomalaa mining area and central Kolaka Regency. The UHI effect was most pronounced from evening to morning, peaking during the night and early morning hours, with increased intensity during the dry season from July to September. Regression analysis revealed a trend of increasing UHI following Urban Sprawl activity, with a trend rate of 0.91°C. The R-squared value of 96.69% indicates that Urban Sprawl activity accounted for 96.69% of the UHI intensity in Kolaka, while other unexamined variables influenced 3.31%.

Introduction

The high rate of development in major cities in Indonesia has led to the phenomenon of Urban Sprawl [1]. This term refers to urban areas expanding into suburban areas [2]. Urban Sprawl occurs due to housing development, new infrastructure, and rapid changes in the transportation system that are not accompanied by the availability of land [3]. According to

the world urbanization prospects 2018, it is projected that by 2050, two-thirds of the global population will reside in urban areas, driven by demographic transitions and population growth [4]. Population projections are scientifically derived calculations based on assumptions regarding the components of population growth rates: births, deaths, and migration [5]. The development of society and the acceleration of urbanization create different land cover patterns, affecting the microclimate in these areas. Urbanization can also trigger changes in the distribution of heat, air humidity, and wind patterns in urban areas, leading to increased convection and atmospheric instability, which cause changes in the intensity of thunderstorms, rainfall, and air temperature on both spatial and temporal scales [6]. Kolaka region has become a target for urbanization and strategic national development as a center for nickel mining production, fishery processing, agriculture, and cocoa plantations. This is evidenced by the population increase in Kolaka Regency by 55,807 people, or 30.1%, from 2010 to 2021 [7], [8].

Kolaka Regency is located at coordinates 3.13° - 4.35° South Latitude and 121.05° - 121.99° East Longitude, with Kolaka District as the urban center (121.611 East, 4.04608 South). This area is considered interesting to study due to the continuous development of Kolaka Regency and the limited availability of open spaces due to industrial activities and sustainable development, potentially leading to changes in air temperature in the urban center and other areas. Urban expansion changes the heat capacity, thermal conductivity, and surface albedo [9], resulting in different energy balances in urban areas compared to other regions [10]. These changes in heat balance cause urban areas to be warmer than other areas, a phenomenon known as Urban Heat Island (UHI) [11]. UHI occurs due to the conversion of vegetated land into layers of concrete, asphalt, high-rise buildings, and other infrastructure to meet the demands and population growth [12].

Urban Sprawl causes changes in air temperature, contributing to the increase in UHI in urban areas [13], [14]. As weather refers to short-term atmospheric conditions[15], UHI significantly influences local temperature patterns, which can affect broader climate trends in urban areas. Numerical Weather Modeling studies allow projections of Urban Sprawl's impact on UHI in urban areas [16], [17]. The Weather Research and Forecasting - Advanced Research WRF (WRF ARW) numerical weather modeling is considered capable of representing the very complex and intricate natural state using numerical equations, which can help provide weather and climate information [18]. WRF has four urban canopy layer schemes: Single layer urban canopy model (SLUCM), computes latent heat flux, sensible heat flux at the surface, and soil surface temperature, offering boundary conditions for lower-level numerical models [19]. Building effect parameterization (BEP) model segments the urban canopy into layers, accounting for interactions between these layers and energy exchanges between buildings and the atmosphere and Building energy model (BEM) model, a variation of BEP, incorporates the effects of air conditioning on local climate, emphasizing more detailed energy exchanges and layer interactions [20]. Non-UCM refers to weather modeling that does not include the urban canopy model. By using a combination of these schemes, the WRF model can provide better estimates of atmospheric conditions in urban environments and their impact on building energy and thermal comfort [21].

This study aims to analyze the air temperature causing UHI using the WRF model with land cover data from the Geospatial Information Agency (BIG) and three types of urban models, SLUCM, BEP, and BEM, and compare them with the default land cover mode or non-UCM (before land modification) of WRF. Furthermore, it aims to analyze the spatial and temporal

characteristics of UHI and the impact of Urban Sprawl on UHI changes in Kolaka Regency using existing non-rainfall events (Table 1) and Urban Sprawl projections by Regent Regulation No. 44 on the Detailed Spatial Plan of the Kolaka Urban Area for 2022-2042. Non-rainfall events are identified from days where no precipitation is recorded across all 8 rain posts in Kolaka. A day is classified as a non-rainfall event if all stations report 0 mm of precipitation; otherwise, it is excluded from the analysis. Kolaka Regency experiences a monsoonal type of rainfall characterized by a single peak in the rainy season. The lowest rainfall occurs in the first dekad of August, while the peak rainfall is observed in the first dekad of April. The dry season lasts for 12 dekads, beginning in the third dekad of July through the second dekad of November, with an average rainfall of less than 50 mm per dekad, followed by the subsequent dekad. The rainy season lasts for 24 dekads, starting from the third dekad of November through the second dekad of July, with an average rainfall exceeding 50 mm per dekad, followed by the next dekad [22]. In this study, a significant novelty is the substitution of the default MODIS-based land cover map with data from the Geospatial Information Agency (BIG) and the integration of urban expansion projections. This approach allows for a more precise and region-specific analysis of UHI dynamics, enhancing the accuracy of the assessment in the Kolaka Regency.

Experimental Method

Data Sources

This research utilized a comprehensive array of data sources to ensure a thorough and accurate analysis of the meteorological conditions and land cover characteristics in Kolaka Regency. The dataset includes primary data such as air temperature and rainfall, as well as secondary data comprising land cover information and Final Analysis data (FNL) as inputs for the WRF model. The data sources employed in this study were employed:

1. Observational and Automatic Weather Station (AWS) air temperature data from Kolaka Meteorological Station, AWS Samaturu and AWS Tanggetada. These observational temperature data are employed to verify the performance of the WRF model. The purpose of this verification process is to assess the model's ability to replicate observed atmospheric conditions and to ensure the reliability of the weather prediction results.
2. Rainfall data from 8 rain posts in Kolaka: Kowioha, Balandete, Tandebura, Induha, Petudua, Kaloloa, Ranojaya, and Kolaka Meteorological Station. This rainfall data is used to determine the non-rainfall days in Kolaka Regency. This approach was chosen to minimize the influence of precipitation, which can significantly affect surface temperature and heat distribution, thereby ensuring a clearer and more reliable analysis of UHI dynamics.
3. Land cover data from the Indonesian Topographic Map (RBI) produced by the Geospatial Information Agency (BIG), in shapefile format, derived from Kolaka Regency Regulation No. 44 of 2022 concerning the Detailed Spatial Plan (RDTR) for the Urban Area of Kolaka Regency 2022-2042. This data is necessary because the WRF model, which uses land cover data from the Moderate Resolution Imaging Spectroradiometer (MODIS) and the United States Geological Survey (USGS), does not accurately reflect the current conditions of Kolaka Regency.This discrepancy arises because the USGS land cover data, developed by the United States Geological Survey, is based on high-resolution global imagery from April 1992 to March 1993, while MODIS data, developed by the University of Boston,

relies on land cover maps derived from Moderate Resolution Imaging Spectroradiometer data from January to December 2001 [23].

4. FNL at the time of the event were used as input data for WRF modeling, with a spatial resolution of 1°×1° (approximately 111 km) and a 6-hour temporal resolution (00:00-00:00 UTC), data downloaded from http://rda.ucar.edu.

Table 1. Illustrates the research data collection time presents the period of non-rainfall days, which refers to specific days selected for data sampling to verify the WRF model. These non-rainfall days were chosen to minimize the influence of precipitation on surface temperature and heat distribution, thereby ensuring a more accurate and reliable model evaluation. Table 1 includes 48 non-rainfall days, divided into 4 samples per month.

Table 1. Research Data Collection Time

January	February	March	April	May	June
01/09/2022	02/04/2022	03/02/2022	04/05/2022	05/03/2022	06/01/2022
01/23/2022	02/23/2022	03/10/2022	04/07/2022	05/11/2022	06/06/2022
01/26/2022	02/27/2022	03/17/2022	04/13/2022	05/15/2022	06/14/2022
01/29/2022	02/28/2022	03/24/2022	04/21/2022	05/28/2022	06/20/2022

July	August	September	October	November	December
07/12/2022	08/04/2022	09/01/2022	10/20/2022	11/03/2022	12/07/2022
07/19/2022	08/11/2022	09/09/2022	10/22/2022	11/17/2022	12/13/2022
07/24/2022	08/15/2022	09/25/2022	10/25/2022	11/21/2022	12/21/2022
07/28/2022	08/19/2022	09/27/2022	10/27/2022	11/25/2022	12/26/2022

Data Application and Processing

Observational and AWS data were used to verify the WRF model output. The RBI BIG land cover data was incorporated as input for the WRF model to represent the current state of Kolaka accurately. The digitized map was digitized and entered into the WRF model using MATLAB software [24]. This step was necessary because the default land cover data in the WRF model, which uses moderate resolution imaging spectroradiometer (MODIS) and United States geological survey (USGS) data, did not accurately reflect the current conditions in Kolaka Regency. The process of map creation and land cover classification conversion followed the methodology employed by Anderson et al. in their research [25] (Figure 1). A single rain gauge represents a 5 km radius around the observation point, whereas air temperature measurements correspond to a 30 km radius around the observation point [26].

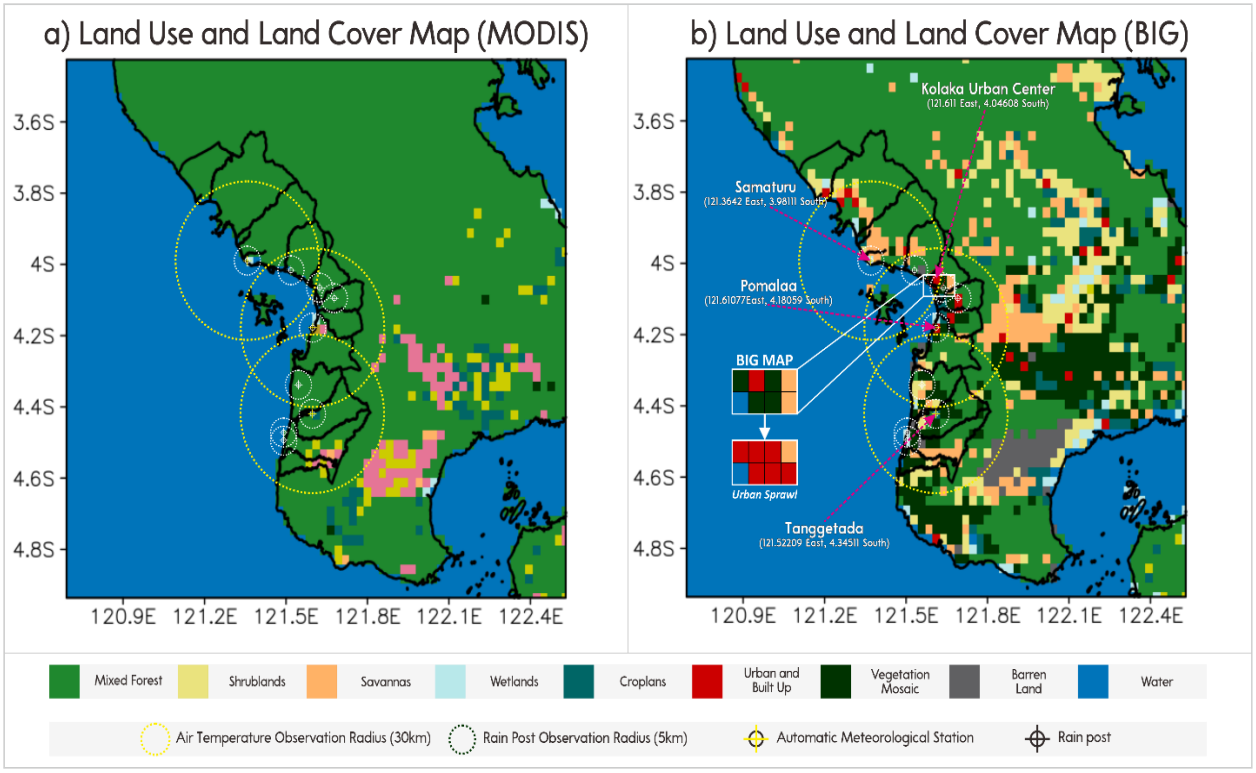

Figure 1. Land Cover Map of Research Area (a) WRF Non-Modified USGS MODIS land cover and (b) WRF model with BIG and Urban Sprawl land cover.

Research Design

In this study, we employed a comparative experimental research model. The comparative method involves comparing observed air temperatures with WRF model outputs. Observational data in this study were sourced from conventional and automatic (AWS) observation instruments. The experimental method involves modifying or manipulating land cover within the WRF model. Data processing in this research utilized ArcGIS, WRF, MATLAB, and GrADS to generate air temperature values and Urban Heat Island (UHI) effects based on land cover manipulations using the RBI BIG Map and Kolaka Regent Regulation No. 44 of 2022, according to predetermined parameterization (Table 2). The study was conducted in 2022, with 48 samples selected yearly. This selection was based on experimental and comparative research requirements, which necessitate a minimum of 30 samples per group [27]. The 48 samples were divided into 4 monthly samples, focusing on conditions without rainfall (Table 1). These were then grouped into observational data, BIG-SLUCM, BIG-BEP, BIG-BEM, and Non-UCM/default WRF model (before land modification) categories.

Table 2. illustrates the parameterization of research presents the configuration of the parameterization schemes used. The downscaling and nesting processes are employed to obtain high-resolution output, allowing for a detailed representation of meteorological phenomena. These processes enable the model to capture finer spatial and temporal details, enhancing its ability to simulate local weather conditions more accurately and effectively.

Table 2. Parameterization of Research

Parameter	Domain 1	Domain 2	Domain 3
Meridional Grid Dimension	96	82	70
Zonal Grid Dimension	82	70	58
Grid Resolution	27 km	9 km	3 km
Terrain Resolution	10 min	5 min	2 min
Micro Physics	WSM 6-class	WSM 6-class	WSM 6-class
Cumulus physics	BMJ	BMJ	BMJ
Boundary Layer	BouLac PBL	BouLac PBL	BouLac PBL
Surface Physics	Noah Land	Noah Land	Noah Land
Urban Surface	SLUCM	SLUCM	SLUCM
	BEP	BEP	BEP
	BEM	BEM	BEM
	Non UCM	Non UCM	Non UCM
History Interval Output	180 min	60 min	60 min

The verification of this research utilized the mean absolute percentage error (MAPE) and Taylor diagram.

MAPE is a commonly employed evaluation metric in forecasting to measure model accuracy. A lower MAPE value indicates better model accuracy [28] (Table 3). The MAPE value can be calculated using the formula in Equation (1).

$$MAPE = \frac{1}{n}\sum_{t=1}^{n}\frac{|S_t - O_t|}{O_t} \quad (1)$$

The verification of this research utilized the mean absolute percentage error (MAPE) and Taylor diagram. Where O_t represents the observed values at time t, S_t denotes the WRF model simulation values at time t, and n is the total number of data periods.

Table 3. The signification of MAPE [28]

MAPE (%)	Signification
< 10	Excellent forecasting ability
10 – 20	Good forecasting ability
20 – 50	Reasonable forecasting ability
> 50	Bad forecasting ability

The Taylor Diagram (Figure 2) is a visual tool used to compare model performance with observational values: the black line is the Standard Deviation (σ), blue line is the correlation coefficient (ρ) and green line is the CRME (E'). This diagram graphically summarizes three statistical metrics: the standard deviation of the WRF model and observations (Equation 2), the correlation coefficient between the WRF model and observations (Equation 3), and the Centered Root Mean Square Error (CRMSE) value (Equation 4) [29]. The Taylor Diagram is expressed by the formula:

$$\sigma = \sqrt{\frac{\sum_{i=1}^{n}(x_i - \bar{x})^2}{n-1}} \quad (2)$$

$$\rho = \frac{\frac{1}{n}\sum_{i=1}^{n}(O_n - \bar{O})(S_n - \bar{S})}{\sigma_O \sigma_S} \quad (3)$$

$$E' = \left\{\frac{1}{n}\sum_{i=1}^{n}[(O_n - \bar{O}) - (S_n - \bar{S})]^2\right\}^{\frac{1}{2}} \quad (4)$$

Where x_i represents each individual data point in the dataset, $\bar{x}$ the mean (average) of all the data points, O is the observation value, S is the simulation value of the WRF model, n is total number of data points or sample size.

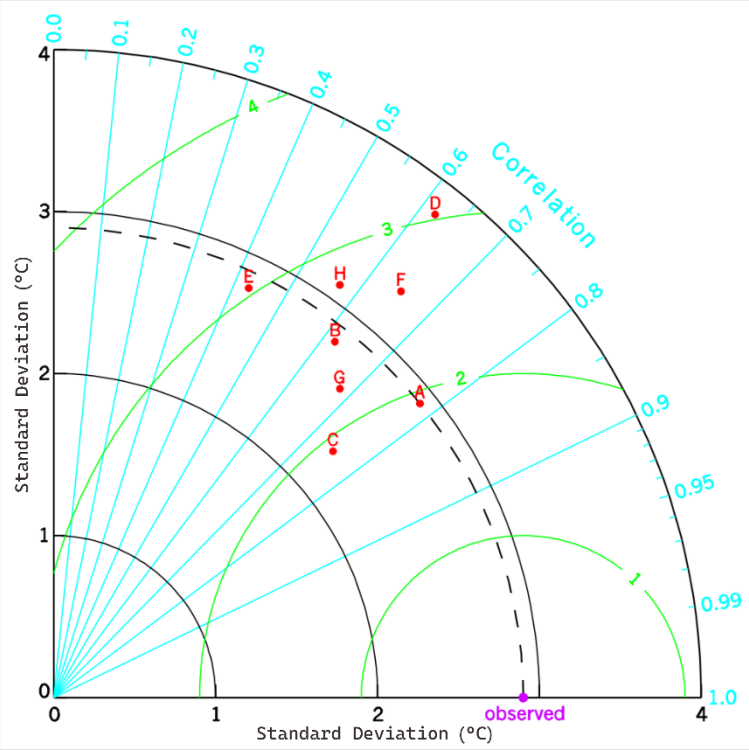

Figure 2. Taylor diagram. [29].

According to research by Velázquez-Ruiz et al. [30] on the assessment of WRF model temperature and rainfall forecasts in the Bahía de Banderas Region (Mexico), the results obtained by the WRF model for air temperature forecasts are considered accurate if they achieve an error margin of less than 2°C and a correlation value of 84%, which is classified as a very strong category [31]. The final stage involves conducting spatial and temporal analysis of the Urban Heat Island (UHI) effect in the Kolaka region for 2022 and its projected changes in 2042 after Urban Sprawl modification, using regression analysis and R Square. For the creation of spatial maps and temporal distribution of UHI, (Equation 5) [32],

$$UHI = T_{mean} - (\mu + 0.5\sigma) \quad (5)$$

where T_{mean} is the land surface air temperature (°C), μ is the mean land surface air temperature (°C), and σ is the standard deviation of land surface air temperature (°C).

Results and Discussion

Figure 3 shows the average MAPE graph comparing observational air temperature and WRF model outputs on an hourly basis over 12 months for the regions of Pomalaa, Tanggetada, and Samaturu. Blue indicates the SLUCM model, Orange the BEP model, Grey the BEM model, and Yellow the Non-UCM model.

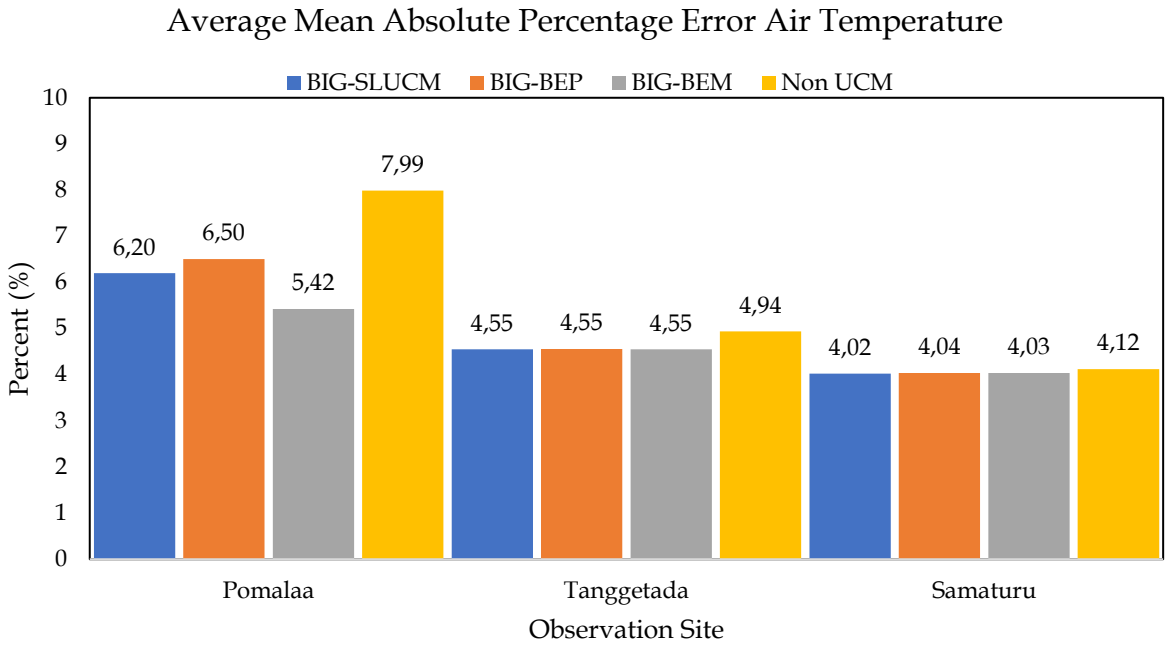

Figure 3. Graph of Average MAPE for Air Temperature in the Pomalaa, Tanggetada, and Samaturu Regions.

Generally, Figure 3. show the air temperature patterns of the four WRF surface models are consistent with the observed air temperature variations. The competency results of the BIG-SLUCM model for the regions of Pomalaa, Tanggetada, and Samaturu were 6.20%, 4.55%, and 6.47%, respectively. BIG-BEP model results for Pomalaa, Tanggetada, and Samaturu were 6.50%, 4.55%, and 4.04%, respectively. BIG-BEM model results for Pomalaa, Tanggetada, and Samaturu were 5.42%, 4.55%, and 4.03%, respectively. Non-UCM model results for Pomalaa, Tanggetada, and Samaturu were 7.50%, 4.55%, and 4.04%, respectively. The model evaluation results (Figure 3) demonstrate Excellent forecasting ability of the WRF model, evidenced by the error range of all four models being below 10% [28]. Over the 12 months, the smallest error was observed in the BIG-BEM model, with an average error range of 4.67%, while the largest error was seen in the non-UCM model, with an average error value of 5.68%.

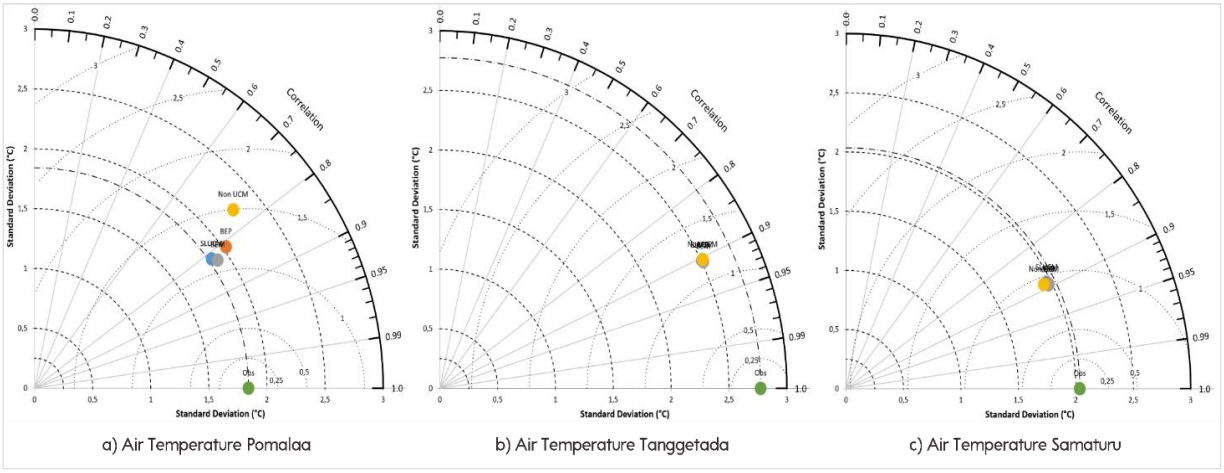

Figure 4. Taylor diagram of regional air temperature (a) Pomalaa, (b) Tanggetada, and (c) Samaturu.

Figure 4 shows the Taylor diagram of regional air temperature Pomalaa, Tanggetada and Samaturu. Blue indicates the SLUCM model, orange represents the BEP model, grey denotes the BEM model, yellow signifies the Non-UCM model, and green represents the observation data. From the diagram, it can be observed that the BIG-BEM model exhibits a very strong to nearly perfect correlation [31], with the lowest CRMSE value among the other models, meeting the criteria for a model to be considered accurate [30]. Specifically, the BIG-BEM model achieves a correlation ranging from 82.74% to 90.62%, with an average of 87.62%, and a CRMSE between 0.90 and 1.18, averaging 1.06. In comparison, the BIG-SLUCM model shows a correlation ranging from 81.61% to 90.40%, with an average of 86.99%, and a CRMSE between 0.92 and 1.18, averaging 1.08. The BIG-BEP model demonstrates a correlation between 81.30% and 90.41%, with an average of 87.05%, and a CRMSE ranging from 0.90 to 1.19, averaging 1.09. Lastly, the non-UCM model shows a correlation ranging from 75.40% to 90.31%, with an average of 84.92%, and a CRMSE between 0.92 and 1.48, averaging 1.18.

Based on research results testing the performance of the best model in identifying air temperature causing UHI using the WRF model with BIG-SLUCM, BIG-BEP, BIG-BEM and non-UCM land cover at three observation points, the average results of the three observation locations show that the BIG-BEM Model has the highest verification value and lowest error. This is evidenced by the lower percentage of MAPE (Figure 3) and CRMSE (Figure 4), and higher Model Correlation value (Figure 4) for BIG-BEM compared to other models (Table 4). The average results of the comparative testing of WRF BIG-SLUCM, BIG-BEP, and BIG-BEM model competencies compared to the non-UCM model from January to December are displayed in Table 4.

Table 4. Average Percentage Comparison of MAPE, Correlation, and CRMSE of BIG Model Model with Non-UCM of Pomalaa, Tangetada and Samaturu regions.

Model	BIG and Non-UCM Model Comparison Percentage			Best Results
	MAPE	Correlation	CRMSE	
SLUCM	13.56%	2.44%	8.47%	
BEP	11.57%	2.50%	7.60%	
BEM	17.92%	3.18%	10.11%	✓

As shown in Table 4, the addition of BIG land cover and the BEM urban scheme demonstrates an improvement in WRF model quality, with a MAPE percentage of 17.92%, correlation of 3.18%, and CRMSE of 10.11% when compared to the default WRF model/non-UCM (before modification with BIG land cover and urban scheme additions). These results align with the research Bhati and Mohan [16] on the performance evaluation of the WRF model and SLUCM land cover model in the Delhi region, India, which showed an increase in RMSE values. However, in the Kolaka region, the WRF BIG-BEM model demonstrates the best model quality compared to the BIG-SLUCM and BIG-BEP models.

Based on the results of the WRF Model Test, the BIG-BEM model was identified as the best-performing model and subsequently applied to the Modeling Influence of Urban Sprawl on UHI Activity in Kolaka Regency. The results are presented as spatial visualizations of the average UHI before and after modifications, along with raster-based temporal comparison graphs of UHI over a 24-hour period before and after modifications (Figures 5–7).

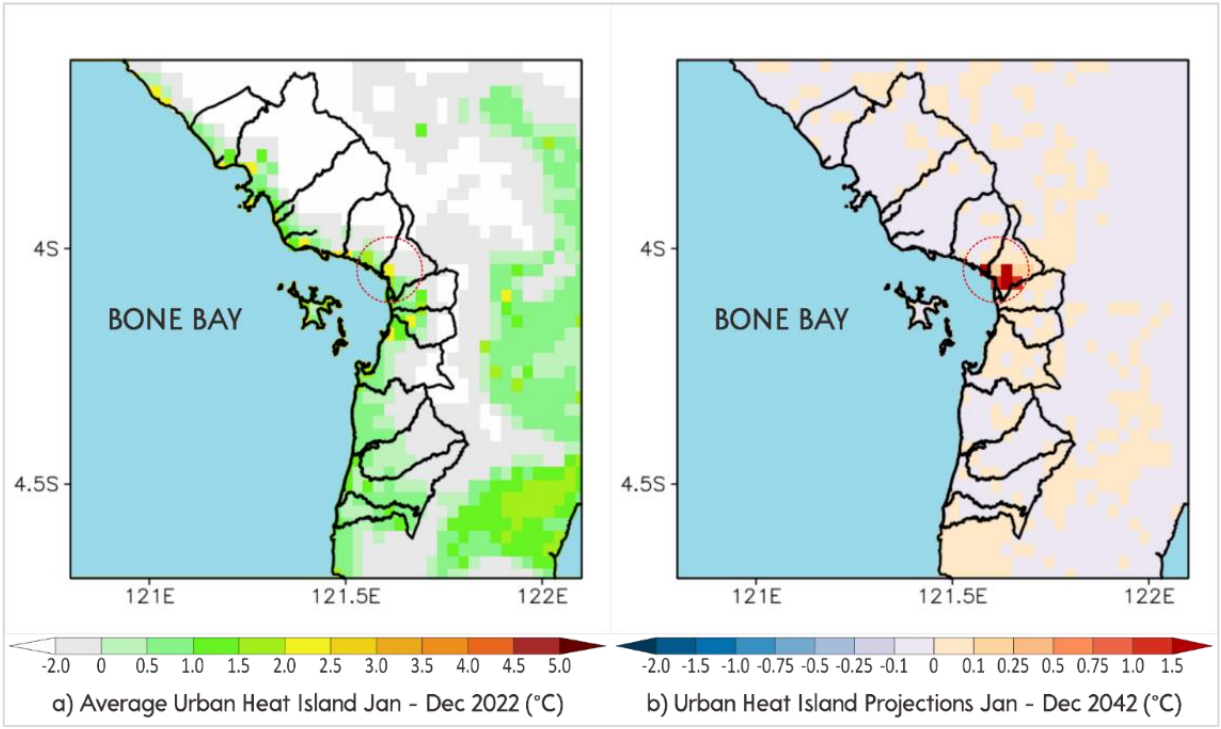

Figure 5. Urban Heat Island January - December (a) Average and (b) Projected

The results obtained by the spatial distribution map of the average UHI in the Kolaka Region from January to December 2022 (Figure 5a), when compared with the BIG land cover of the Kolaka region (Figure 1), show that the UHI in Kolaka is predominantly in the range of -2.0°C to 2.5°C. The Pomalaa mining area and the center of Kolaka Regency (Red Circle) exhibit the highest UHI class range of 1.5°C to 2.5°C. The development of the Kolaka region is dominated by settlements in the western area (Bone Bay Coast) with a UHI range of 0.5°C to 1.5°C, while the eastern region of Kolaka (protected forest land cover) has UHI values below 0°C. This aligns with studies [12], [33], [34] showing that UHI forms when vegetation is replaced by asphalt, concrete, buildings, and other infrastructure. These altered ground surfaces absorb

and reflect more solar heat, leading to increased surface temperatures. The conversion of vegetation to concrete, asphalt, or open land causes an increase in diurnal temperature, which ultimately affects the climatological temperature.

The projected change in average UHI after Urban Sprawl from January to December 2042 (Figure 5b), when compared with the BIG land cover of the Kolaka region (Figure 1), shows an increase in UHI values in the Urban Sprawl area (Red Circle) ranging from 0.5°C to more than 1.5°C. This change occurs due to the blocking effect from the expanding urban area. The blocking effect refers to situations where tall or uniquely shaped buildings obstruct surrounding air flow. This can cause hot air to be trapped around buildings, leading to increased temperatures in the surrounding environment. This is consistent with research [13] showing that the intensity and frequency of air temperature due to urbanisation continue to increase as urban areas grow larger. Figure 6 displays a raster graph of the average UHI characteristics derived from the WRF BIG-BEM model output from January to December 2022

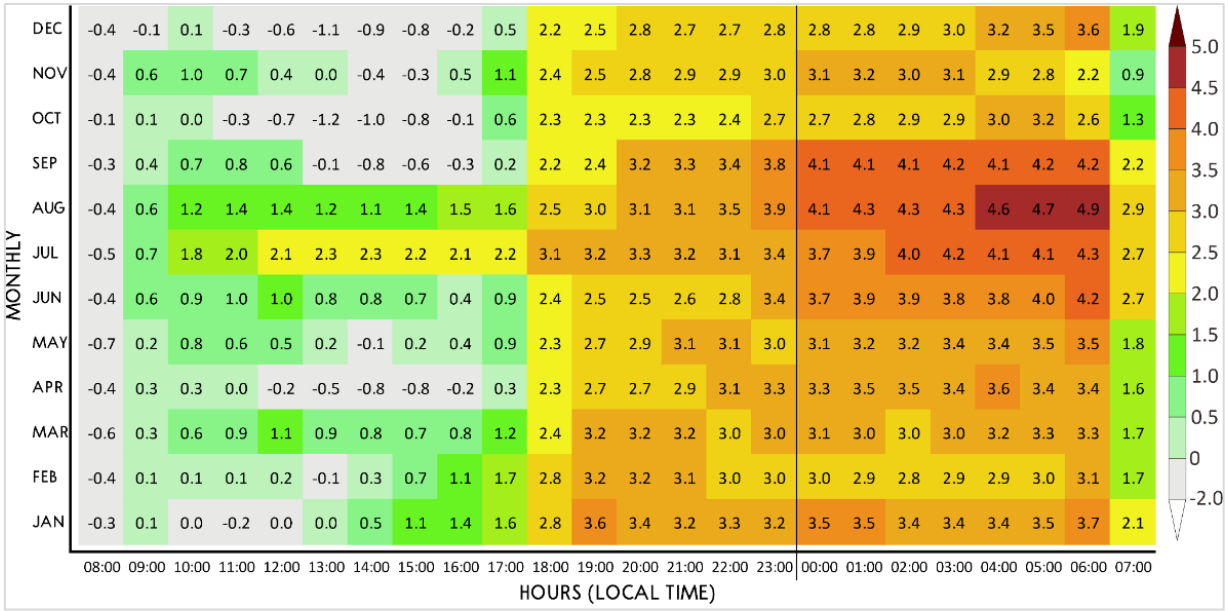

Figure 6. Raster graph of mean UHI of BIG-BEM WRF model output (°C) for January - December 2022.

Figure 6. shows that UHI increase is predominantly observed from late afternoon to early morning, with peak UHI occurring from night to early dawn. This UHI intensification occurs because the urban areas of Kolaka, consisting of layers of asphalt, concrete, and cement, absorb and retain more heat. During the day, these materials absorb solar heat, which is then released into the surrounding air at night. Furthermore, human activities such as car use, indoor heating, and Kolaka's nickel mining industry, which continues through the night, generate additional heat, causing the UHI distribution to continue increasing from night to early morning. This aligns with studies [35], [36] which state that urban materials cannot efficiently release the heat accumulated during the day. Consequently, temperatures in the city remain high at night, whereas rural areas with more vegetation and open soil can cool more effectively through radiation processes.

UHI can occur throughout the year; however, its intensity can increase during the dry season in the Kolaka region from July to September (Figure 6). During this period, the already dry soil has a lower capacity to absorb water and a reduced evaporation rate, which can lead to increased temperatures in urban areas [37], [38]. Human activities in the Kolaka region, which generate additional heat, can also contribute to the temperature rise during the dry season. Figure 7 displays a raster graph of the average UHI characteristics derived from the WRF model output after urban sprawl modification for January to December 2042

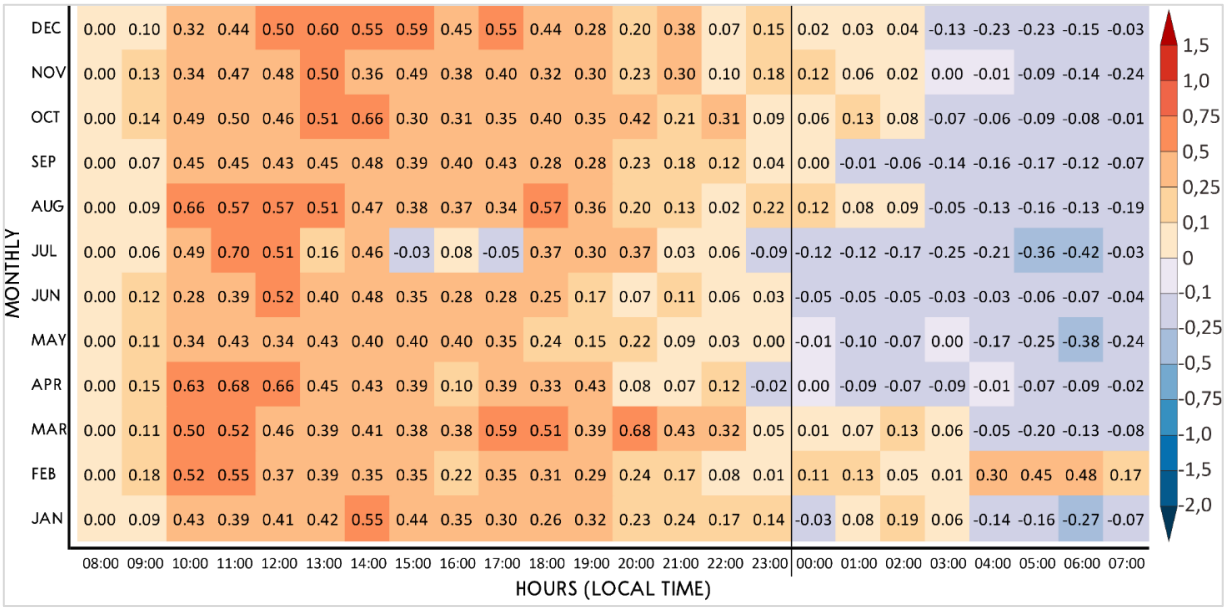

Figure 7. Raster graph of mean UHI of WRF model output (°C) after Urban Sprawl modification in January - December 2042.

Figure 7. shows that UHI increase is predominantly observed from morning to afternoon, with a decrease in UHI during the early hours. The increase in UHI from morning to afternoon occurs due to the blocking effect of buildings, which causes hot air to be trapped around the structures, leading to increased temperatures in the surrounding environment [39]. Conversely, the decrease in UHI difference at night in Kolaka's urban center is attributed to the transformation of previously vegetated surrounding areas into built-up areas [40]. This phenomenon occurred because, in 2022, Kolaka urban center (121.611 East, 4.04608 South) exhibited a high UHI effect, being the only urbanized area while the surrounding regions consisted mostly of a mosaic of vegetation and savannas. The urban area absorbed more heat compared to other land covers (red circle) [33], resulting in higher temperatures in urban center relative to its surroundings (Figure 5a). However, by 2042, as the previously vegetated and savanna-covered regions underwent urban sprawl (Figure 1b), the temporal UHI in urban center showed a relative decrease from early morning until dawn (Figure 7). This suggests that widespread urban sprawl can lead to a more even distribution of heat across the urban landscape, making the urban center no longer the sole heat reservoir for surface temperatures (Figure 5b) [40].

The projected change in average UHI after urban sprawl from January to December 2042 (Figure 7), when compared with the BIG land cover of the Kolaka region (Figure 1b), shows

an increase in UHI values in the urban sprawl area (Red Circle) ranging from 0.5 to more than 1.5°C. This change occurs due to the blocking effect from the expanding urban area (Figure 8).

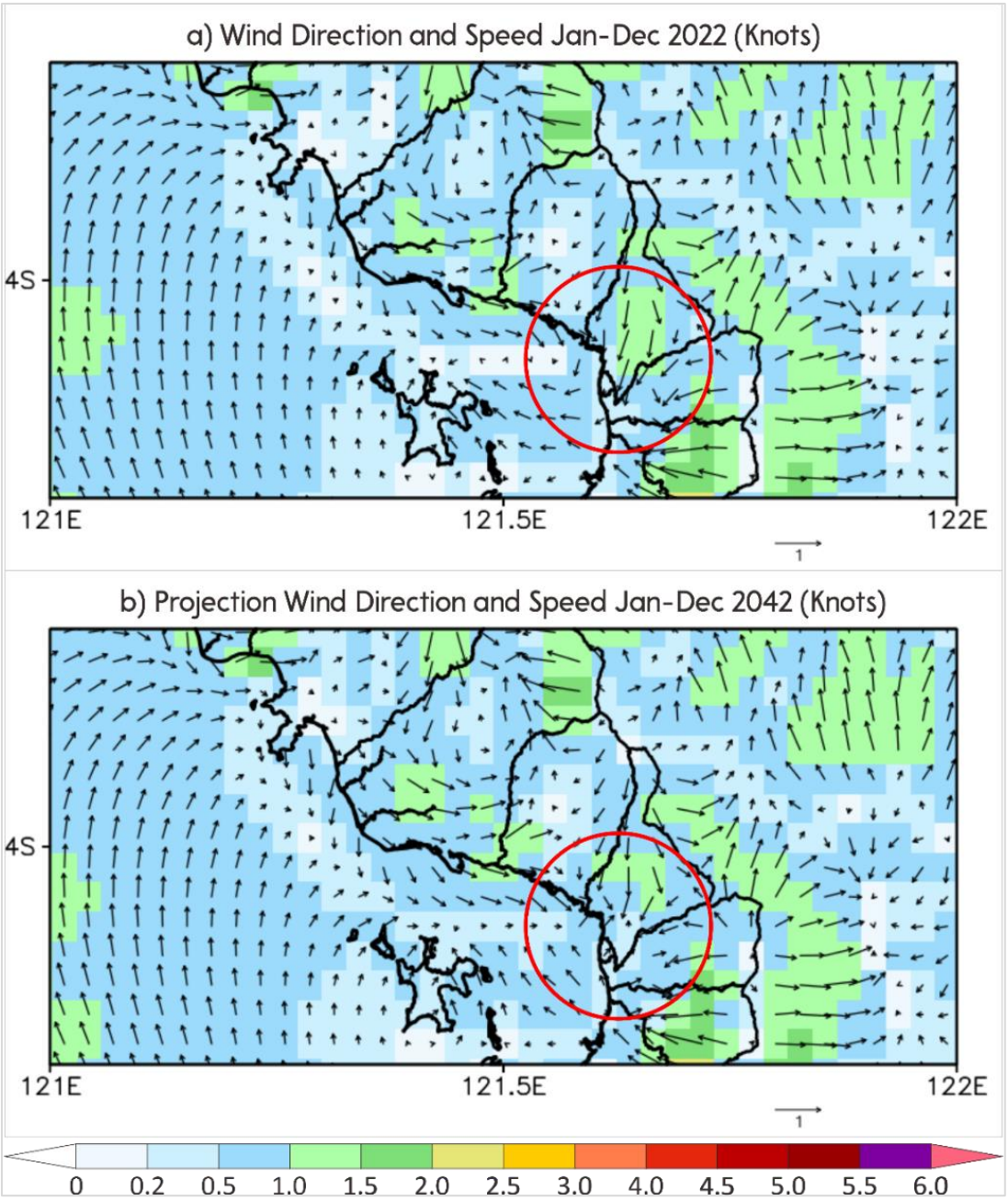

Figure 8. Kolaka Region Wind Direction and Speed (Knots) (a) BIG-BEM 2022 Model and (b) BIG-BEM and Modified Urban Sprawl 2042 Model.

Figure 8 illustrates the deviation and reduction of wind speed as it interacts with urban geometries. This change occurs due to the blocking effect from the expanding urban area, specifically at coordinates 121.638 East and 4.07307 South (Figure 8b). This occurs because the direction and velocity of wind depend on geometric variables related to the building's shape [41], [42]. When wind flows past a building, it may spread or deviate from its original path. The building's shape can block or deflect the wind, resulting in a reduction of wind speed. If

there are other buildings in close proximity to the main building, creating a sheltered zone behind the building becomes challenging. These nearby buildings can disturb and alter the wind direction, thus preventing the formation of such sheltered zones [39]. The phenomenon of blocking in buildings and the resulting increase in surrounding air temperature can be explained by physical laws related to heat radiation and energy transfer, as well as the Coandă effect, which describes fluid flow following the curvature of an object. The Coandă effect causes air flow to follow the surface of buildings, creating blocked or obstructed zones [43].

The changes in UHI values for Kolaka Regency in 2022 (Before Modification, Figure 6) and in 2042 (After Urban Sprawl, Figure 7) are shown in Figure 9, which presents a Linear Regression Graph of UHI outputs from the BIG-BEM WRF model before and after the modification of urban expansion.

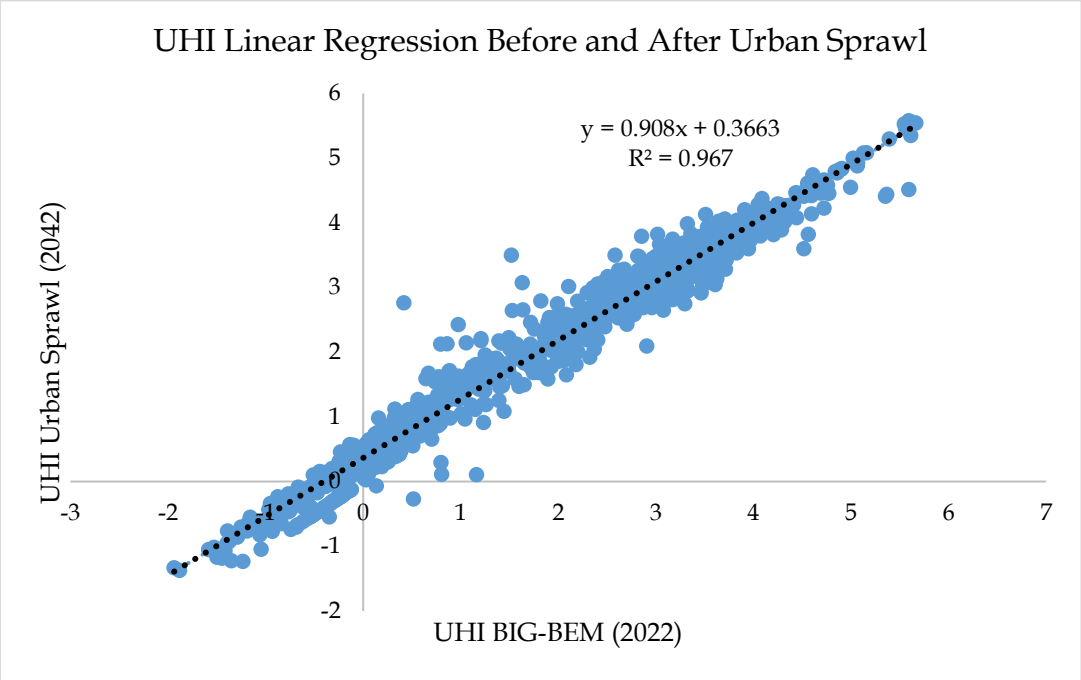

Figure 9. Linear Regression Graph of UHI of BIG-BEM WRF model output before and after Urban Sprawl Modification.

Figure 9 reveals that 24 out of 48 UHI samples experienced an increase in the UHI peak values, highlighting the significant impact of urban sprawl on local temperatures. The regression analysis of the 48 UHI samples further indicates a consistent upward trend in UHI intensity in 2042, following the ongoing urban sprawl, with an average increase of 0.91°C. This increase in UHI intensity is a direct consequence of urban expansion, as more urbanized areas replace natural land cover, leading to higher surface temperatures. The R-Square value obtained, which is in the range of 0.97, suggests a very strong correlation between urban sprawl and UHI intensity, indicating that 96.69% of the variation in UHI intensity in the Kolaka region during non-rainy days can be attributed to urban sprawl activities. This suggests that urban sprawl plays a dominant role in shaping the local climate. However, the remaining 3.31% of UHI intensity is influenced by other variables that were not included in the scope of this study,

such as atmospheric conditions, land use changes in neighboring areas, and other potential microclimatic factors that may affect the UHI phenomenon in Kolaka.

The increase in UHI intensity is consistent with the findings of Y. Wang et al. [44], which show that the intensity and frequency of extreme high temperatures in major BTH cities have risen significantly, with an average rate of 0.15°C−1°C per decade over a 25-year period. This aligns with IPCC projections, which predict a global average temperature rise of 1.8°C–4.0°C in urban areas by 2100 [45]. The intensification of UHI is known to have detrimental effects on human health, ranging from dehydration and heat stress to heat stroke [41]. Additionally, elevated UHI intensity can exacerbate pre-existing cardiovascular, respiratory, and kidney conditions, particularly in vulnerable populations such as the elderly and children [46], [47].

Conclusion

The usage of the WRF model with BIG-BEM configuration exhibits the highest verification scores and the lowest errors. Incorporating BIG land cover and BEM urban schemes also demonstrates an enhancement in WRF modeln compared to the default WRF model (prior to incorporating BIG land cover and urban scheme). The highest UHI intensity is found in Pomalaa's mining areas and Kolaka's urban center, while protected forests have the lowest values. UHI peaks at night to early morning, with notable increases during the dry season (July–September). The influence of urban sprawl on UHI activity indicates a projected increase in UHI intensity by 2042, with a trend rate of 0.91°C. Urban sprawl triggers a blocking effect that hampers air circulation and traps heat around buildings, thereby contributing to temperature increases in the surrounding environment.

Suggestion

The recommendations for urban development in the Kolaka region to mitigate the impact of increased Urban Heat Island (UHI) effects, based on the research findings, are as follows:

1. Avoid the densification of new building developments in areas where the blocking effect occurs, particularly at the coordinates 121.638 East and 4.07307 South.
2. Utilize building materials with high reflectivity to minimize heat absorption from sunlight and reduce the surface temperatures of buildings that become trapped due to the wind-blocking effect, especially if the area continues to experience development compaction due to construction.

Acknowledgment

Acknowledgments are extended to the Department of Public Works and Spatial Planning of Kolaka Regency for providing the land cover map for Kolaka's 2042 development plan. Special thanks to the research supervisors for their invaluable guidance and for imparting new insights and understanding regarding the urban climate.

References

[1] F. Hanief and S. P. Dewi, 'Pengaruh Urban Sprawl Terhadap Perubahan Bentuk Kota Semarang Ditinjau dari Perubahan Kondisi Fisik Kelurahan Meteseh Kecamatan Tembalang', *J. Perenc. Wil. dan Kota Fak. Tek. Univ. Diponegoro*, vol. 2, no. 1, pp. 341–350, 2014, doi: https://ejournal3.undip.ac.id/index.php/ruang/article/view/4367/5124.

[2] R. Mujiandari, 'Perkembangan Urban Sprawl Kota Semarang pada Wilayah Kabupaten

Demak Tahun 2001-2012', *J. Wil. dan Lingkung.*, vol. 2, no. 2, p. 129, Aug. 2014, doi: 10.14710/jwl.2.2.129-142.

[3] M. Zerhouny, A. Fadil, and M. Hakdaoui, 'Underground Space Utilization in the Urban Land-Use Planning of Casablanca (Morocco)', *Land*, vol. 7, no. 4, p. 143, Nov. 2018, doi: 10.3390/land7040143.

[4] U. Nation, *World Urbanization Prospects 2018*. New York: Department of Economic and Social Affairs Population Division, United Nations, 2019. [Online]. Available: https://population.un.org/wup/

[5] BPS, *Proyeksi Penduduk Indonesia 2020–2050 Hasil Sensus Penduduk 2020*. Jakarta: Badan Pusat Statistik, 2023. [Online]. Available: https://www.bps.go.id/id/publication/2023/05/16/fad83131cd3bb9be3bb2a657/proyeksi-penduduk-indonesia-2020-2050-hasil-sensus-penduduk-2020.html

[6] S. Huang *et al.*, 'Urbanization Amplified Asymmetrical Changes of Rainfall and Exacerbated Drought: Analysis Over Five Urban Agglomerations in the Yangtze River Basin, China', *Earth's Futur.*, vol. 11, no. 2, pp. 1–22, 2023, doi: 10.1029/2022EF003117.

[7] BAPPENAS, *Seri Analisis Pembangunan Wilayah Provinsi Sulawesi Tenggara 2015*. Sulawesi Tenggara: SIMREG BAPPENAS, 2015.

[8] BPS Kolaka, *Kabupaten Kolaka Dalam Angka 2022*. Kabupaten Kolaka: Badan Pusat Statistik Kab. Kolaka, 2022.

[9] H. M. Imran, J. Kala, A. W. M. Ng, and S. Muthukumaran, 'Impacts of future urban expansion on urban heat island effects during heatwave events in the city of Melbourne in southeast Australia', *Q. J. R. Meteorol. Soc.*, vol. 145, no. 723, pp. 2586–2602, 2019, doi: 10.1002/qj.3580.

[10] Z. Yang, F. Dominguez, H. Gupta, X. Zeng, and L. Norman, 'Urban effects on regional climate: A case study in the phoenix and tucson "sun corridor"', *Earth Interact.*, vol. 20, no. 20, pp. 1–25, 2016, doi: 10.1175/EI-D-15-0027.1.

[11] H. K. Jabbar, M. N. Hamoodi, and A. N. Al-Hameedawi, 'Urban heat islands: a review of contributing factors, effects and data', *IOP Conf. Ser. Earth Environ. Sci.*, vol. 1129, no. 1, p. 012038, Jan. 2023, doi: 10.1088/1755-1315/1129/1/012038.

[12] S. P. Darlina, B. Sasmito, and B. D. Yuwono, 'Analisis Fenomena Urban Heat Island Serta Mitigasinya', *J. Geod. Undip*, vol. 7, pp. 109–119, 2018.

[13] Y. Wang, Y. Xiang, L. Song, and X. Z. Liang, 'Quantifying the contribution of urbanization to summer extreme high-temperature events in the Beijing–Tianjin–Hebei Urban agglomeration', *J. Appl. Meteorol. Climatol.*, vol. 61, no. 6, pp. 669–683, 2022, doi: 10.1175/JAMC-D-21-0201.1.

[14] M. Zhao, H. Cai, Z. Qiao, and X. Xu, 'Influence of urban expansion on the urban heat island effect in Shanghai', *Int. J. Geogr. Inf. Sci.*, vol. 30, no. 12, pp. 2421–2441, 2016, doi: 10.1080/13658816.2016.1178389.

[15] K. N. A. Dewi, S. Bhari, and Irwansyah, 'Model Prediksi Curah Hujan Harian Menggunakan Jaringan Syaraf Tiruan Backpropagation', *Indones. Phys. Rev.*, vol. 2, no. 1, pp. 9–17, 2019, doi: 10.29303/i pr.v2i1.17.

[16] S. Bhati and M. Mohan, 'WRF model evaluation for the urban heat island assessment under varying land use/land cover and reference site conditions', *Theor. Appl. Climatol.*, vol. 126, no. 1–2, pp. 385–400, 2016, doi: 10.1007/s00704-015-1589-5.

[17] R. G. J. P. Bilang, A. C. Blanco, J. A. S. Santos, and L. M. P. Olaguera, 'Simulation of Urban Heat Island during a High-Heat Event Using WRF Urban Canopy Models: A Case Study for Metro Manila', *Atmosphere (Basel).*, vol. 13, no. 10, 2022, doi: 10.3390/atmos13101658.

[18] T. W. Hadi, I. D. G. A. Junnaedhi, L. I. Satrya, M. P. Anugrah, and D. T. Octarina, *Pelatihan Model WRF (Weather Research and Forecasting)*. Bandung: Fakultas Ilmu dan Teknologi Kebumian ITB, 2011.

[19] H. Kusaka and F. Kimura, 'Coupling a single-layer urban canopy model with a simple atmospheric model: impact on urban heat island simulation for an idealized case', *J. Meteorol. Soc. Japan*, vol. 82, no. 1, pp. 67–80, 2004, doi: 10.2151/jmsj.82.67.

[20] T. Liang *et al.*, 'Simulation of the influence of a fine-scale urban underlying surface on the urban heat island effect in Beijing', *Atmos. Res.*, vol. 262, no. July, p. 105786, 2021, doi: 10.1016/j.atmosres.2021.105786.

[21] NCAR, *Wrf arw version 3 modeling system user ' s guide april 2016*, no. January. Mesoscale & Microscale Meteorology Division National Center for Atmospheric Research, 2016.

[22] BMKG, *Peta Rata-rata Curah Hujan dan Hari Hujan Periode 1991-2020 Indonesia*. Jakarta: Pusat Informasi Perubahan Iklim BMKG, 2021.

[23] J. Siewert and K. Kroszczynski, 'Evaluation of High-Resolution Land Cover Geographical Data for the WRF Model Simulations', *Remote Sens.*, vol. 15, no. 9, 2023, doi: 10.3390/rs15092389.

[24] H. D. Laksono, *Pengantar Pemograman Dengan Matlab (Aplikasi Pada Matematika Rekayasa)*. Padang: LPTIK Uniiversitas Andalas, 2017.

[25] J. R. Anderson, E. E. Hardy, J. T. Roach, and R. E. Witmer, 'A land use and land cover classification system for use with remote sensor data', *Geol. Surv. Prof. Pap.*, no. 964, 1976.

[26] K. G. Hubbard, 'Spatial variability of daily weather variables in the high plains of the usa', *Agric. For. Meteorol.*, vol. 68, no. 1–2, pp. 29–41, 1994, doi: 10.1016/0168-1923(94)90067-1.

[27] G. E. Mills and L. R. Gay, *Educational research : competencies for analysis and applications*, 11 th. New Jersey: Pearson Education Inc, 2016.

[28] P. C. Chang, Y. W. Wang, and C. H. Liu, 'The development of a weighted evolving fuzzy neural network for PCB sales forecasting', *Expert Syst. Appl.*, vol. 32, no. 1, pp. 86–96, 2007, doi: 10.1016/j.eswa.2005.11.021.

[29] K. E. Taylor, 'Summarizing multiple aspects of model performance in a single diagram', *J. Geophys. Res.*, vol. 106, pp. 7183–7192, 2001, doi: https://doi.org/10.1029/2000JD900719.

[30] A. Velázquez-Ruiz, M. C. Rodríguez-Uribe, F. M. Carrillo-González, J. C. Morales-Hernández, B. Cruz-Romero, and M. L. Bravo-Olivas, 'Assessment of temperature and precipitation forecasts of the wrf model in the Bahía de Banderas Region (Mexico)', *Atmosphere (Basel).*, vol. 13, no. 8, 2022, doi: 10.3390/atmos13081220.

[31] D. A. De Vaus, *Surveys in social research, 5th edition (social research today series)*. London:

Allen & Unwin, 2002. doi: https://doi.org/10.4324/9780203501054.

[32] A. Y. Pratiwi and L. M. Jaelani, 'Analisis Perubahan Distribusi Urban Heat Island (UHI) di Kota Surabaya Menggunakan Citra Satelit Landsat Multitemporal', *J. Tek. ITS*, vol. 9, no. 2, 2020, doi: 10.12962/j23373539.v9i2.53982.

[33] A. Delarizka, B. Sasmito, and Hani'ah, 'Analisis Fenomena Pulau Bahang (Urban Heat Island) di Kota Semarang Berdasarkan Hubungan Antara Perubahan Tutupan Lahan Dengan Suhu Permukaan Menggunakan Citra Multi Temporal Landsat', *J. Geod. Undip*, vol. 5, pp. 188–195, 2016.

[34] M. R. Khomarudin, 'Mendeteksi Pulau Panas (Heat Island) dengan Data Satelit Penginderaan Jauh', *War. LAPAN*, vol. 2, 2004.

[35] A. P. Larasati, B. Rahman, and J. Kautsary, 'Pengaruh Perkembangan Perkotaan Terhadap Fenomena Pulau Panas (Urban Heat Island)', *J. Kaji. Ruang*, vol. 2, no. 1, p. 35, 2022, doi: 10.30659/jkr.v2i1.20469.

[36] H. Muzaky and L. M. Jaelani, 'Analisis Pengaruh Tutupan Lahan terhadap Distribusi Suhu Permukaan: Kajian Urban Heat Island di Jakarta, Bandung dan Surabaya', *J. Penginderaan Jauh Indones.*, vol. 1, no. 2, pp. 45–51, 2019, [Online]. Available: http://jurnal.mapin.or.id/index.php/jpji/article/view/14

[37] P. Kabano, A. Harris, and S. Lindley, 'Spatiotemporal dynamics of urban climate during the wet-dry season transition in a tropical African city', *Int. J. Biometeorol.*, vol. 66, no. 2, pp. 385–396, 2022, doi: 10.1007/s00484-020-02061-1.

[38] A. R. dos Santos *et al.*, 'Spatial and temporal distribution of urban heat islands', *Sci. Total Environ.*, vol. 605–606, pp. 946–956, 2017, doi: 10.1016/j.scitotenv.2017.05.275.

[39] E. Turkbeyler, R. Yao, R. Nobile, T. Bentham, and D. Lim, 'The impact of urban wind environments on natural ventilation', *Int. J. Vent.*, vol. 11, no. 1, pp. 17–28, 2012, doi: 10.1080/14733315.2012.11683967.

[40] J. Zhang, G. Jiao, Q. Ye, and X. Gu, 'The Impact of Urban Expansion on the Urban Thermal Environment: A Case Study in Nanchang, Jiangxi, China', *Sustain.*, vol. 14, no. 24, 2022, doi: 10.3390/su142416531.

[41] O. S. Asfour, 'Prediction of wind environment in different grouping patterns of housing blocks', *Energy Build.*, vol. 42, no. 11, pp. 2061–2069, 2010, doi: 10.1016/j.enbuild.2010.06.015.

[42] N. Serteser and V. Ok, 'The Effects Of Building Parameters On Wind Velocity And Air-Flow Type In The Urban Settlements', *seventh Int. Conf. urban Clim.*, vol. 29, no. June, 2009.

[43] M. Trancossi, 'An overview of scientific and technical literature on Coanda effect applied to nozzles', *SAE Tech. Pap.*, no. May, 2011, doi: 10.4271/2011-01-2591.

[44] Y. Wang, Y. Xiang, L. Song, and X. Z. Liang, 'Quantifying the contribution of urbanization to summer extreme high-temperature events in the Beijing–Tianjin–Hebei Urban Agglomeration', *J. Appl. Meteorol. Climatol.*, vol. 61, no. 6, pp. 669–683, 2022, doi: 10.1175/JAMC-D-21-0201.1.

[45] S. ann Robinson, 'Climate change adaptation in SIDS: A systematic review of the literature pre and post the IPCC Fifth Assessment Report', *Wiley Interdiscip. Rev. Clim. Chang.*, vol.

11, no. 4, pp. 1–21, 2020, doi: 10.1002/wcc.653.

[46] A. Piracha and M. T. Chaudhary, 'Urban air pollution, urban heat island and human health: a review of the literature', *Sustain.*, vol. 14, no. 15, 2022, doi: 10.3390/su14159234.

[47] N. Yadav, K. Rajendra, A. Awasthi, and C. Singh, 'Systematic exploration of heat wave impact on mortality and urban heat island: A review from 2000 to 2022', *Urban Clim.*, vol. 51, no. September, p. 101622, 2023, doi: 10.1016/j.uclim.2023.101622.